Neutron Scattering Study of Novel Magnetic Order in $Na_{0.5}CoO_2$

G. Gašparović,[1] R. A. Ott,[1] J.-H. Cho,[1,3] F. C. Chou,[2] Y. Chu,[1,2] J. W. Lynn,[4] and Y. S. Lee[1,2]

[1]*Department of Physics, Massachusetts Institute of Technology, Cambridge, Massachusetts 02139, USA*
[2]*Center for Materials Science and Engineering, Massachusetts Institute of Technology, Cambridge, Massachusetts 02139, USA*
[3]*RCDAMP and Department of Physics, Pusan National University, Busan 609-735, Korea*
[4]*NIST Center for Neutron Research, Gaithersburg, Maryland 20899, USA*

(Received 5 August 2005; published 31 January 2006)

We report polarized and unpolarized neutron scattering measurements of the magnetic order in single crystals of $Na_{0.5}CoO_2$. Our data indicate that below $T_N = 88$ K the spins form a novel antiferromagnetic pattern within the CoO_2 planes, consisting of alternating rows of ordered and nonordered Co ions. The domains of magnetic order appear to be closely coupled to the domains of Na ion order, consistent with such a twofold symmetric spin arrangement. Magnetoresistance and anisotropic susceptibility measurements further support this model for the electronic ground state.

DOI: 10.1103/PhysRevLett.96.046403 PACS numbers: 74.70.−b, 71.27.+a, 75.25.+z

The layered cobaltates Na_xCoO_2 have attracted much attention because of their unusual thermoelectric properties [1,2] and because of the recent discovery of superconductivity in the hydrated composition [3]. The Co ions in these compounds form a hexagonal lattice, and the average valence can be changed by varying the Na concentration x. The Co^{4+} ions can formally be regarded as magnetic ions with $S = \frac{1}{2}$ on a frustrated low-dimensional lattice. It is believed that strong electronic correlations play an important role in the physics, and, as a function of the Na concentration, a rich phase diagram has been reported [4]. For $x < \frac{1}{2}$, the material is a paramagnetic metal, while for $x > \frac{1}{2}$ an unusual "Curie-Weiss metallic" phase is observed. At $x = \frac{1}{2}$, a unique state is realized: the Na ions are chemically ordered to form zigzag chains in an orthorhombic superstructure with twofold symmetry [5,6], and it has been speculated that this leads to $Co^{3.5+\delta}/Co^{3.5-\delta}$ charge order within each CoO_2 layer [4,7–10]. The ground state is believed to be a magnetically ordered insulator; resistivity, Hall coefficient, thermal transport [4], and angular magnetoresistance oscillation measurements [11] are all consistent with such a twofold symmetric ground state.

In order to further investigate the electronic ground state of the half-doped CoO_2 plane, we have performed neutron scattering, susceptibility, and transport studies on single crystal samples. The combination of polarized and unpolarized neutron scattering data allow us to determine the ordered spin direction and arrangement. We find that the ground state is well described by an ordered array of stripes of antiferromagnetic spins interleaved with stripes of nonordered Co ions.

The samples used in this study were prepared by electrochemically deintercalating a floating-zone grown Na_xCoO_2 crystal to yield a final concentration of $x = 0.5$ [12,13]. Figure 1 shows measurements of the bulk properties of the resulting $Na_{0.5}CoO_2$ crystals. In Fig. 1(a), we plot the in-plane resistivity (ρ_{ab}) measured using the conventional four-probe method on a crystal with dimensions $1 \times 0.5 \times 0.05$ mm^3 in zero applied field. The resistivity dramatically increases below 51 K, consistent with previously published data [4]. The application of a 14 T magnetic field affects ρ_{ab} in different ways depending on the field orientation, as shown in Fig. 1(b). For $H \parallel ab$, a negative magnetoresistance is observed below ~51 K, consistent with previous work by Balicas *et al.* [11]. The kink in the data near 50 K is caused by a shift in the onset temperature of the resistivity upturn. A new observation is that, for $H \parallel c$, the data exhibit a positive magnetoresistance below 88 K. As we discuss further below, this behavior coincides with the magnetic phase transition at $T_N = 88$ K and is consistent with our proposed ground

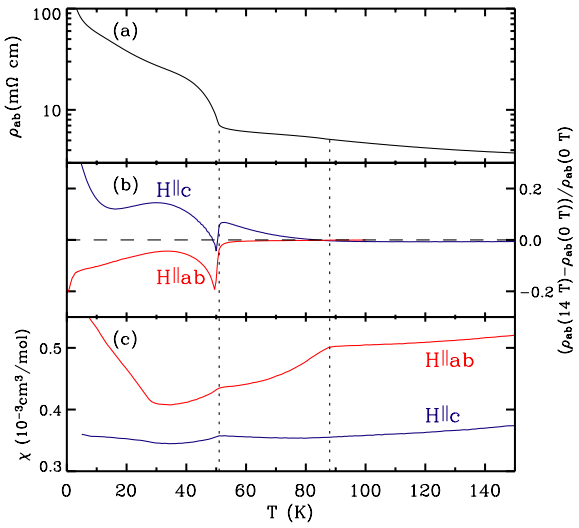

FIG. 1 (color online). Bulk physical properties measured using $Na_{0.5}CoO_2$ single crystals. (a) In-plane resistivity ρ_{ab}. (b) Fractional change of ρ_{ab} measured in a magnetic field of 14 T with $H \parallel c$ and $H \parallel ab$. (c) Anisotropic magnetic susceptibility in a field of 1 T. The vertical dashed lines denote the temperatures of $T = 51$ K and $T_N = 88$ K.

state. The magnetic susceptibility [Fig. 1(c)] is anisotropic and exhibits kinks at $T = 88$ and 51 K [14,15].

Our neutron scattering experiments were conducted at the NIST Center for Neutron Research using the BT9 and BT2 triple-axis spectrometers. The incident and final energies were fixed at 14.7 meV, with collimations 40′-40′-sample-60′-open, resulting in an energy resolution of ~1 meV. Pyrolytic graphite filters were placed in the beam before the sample to reduce higher order neutron contamination. For the polarized measurements, Heusler crystals were used for the monochromator and analyzer, and polarization guide fields were created at the sample position using Helmholtz coils (a flipping ratio of ~21 was achieved). The crystal studied was cylindrically shaped, with mass 2.41 g and a mosaic of 1° to 2° (full width at half maximum), depending on the orientation. The temperature was controlled using a ^{4}He closed cycle refrigerator. We label reciprocal-space peaks using the hexagonal $P6_3/mmc$ space group, with low temperature lattice parameters $a = 2.816$ Å and $c = 11.05$ Å. In $Na_{0.5}CoO_2$, Na ion ordering leads to an orthorhombic supercell ($a_o = \sqrt{3}a$ and $b_o = 2a$) in real space, which produces nuclear superlattice reflections in reciprocal space, such as at $(\frac{1}{2}\ 0\ L)$ and $(\frac{1}{2}\ \frac{1}{2}$ even) [5].

Figure 2 shows evidence for magnetic order below $T_N = 88$ K, obtained by elastic neutron scattering. At low temperatures, new peaks arise that are distinct from the Na superlattice reflections. In the (HHL) zone, we observe such peaks at $\vec{Q} = (\frac{1}{2}\ \frac{1}{2}$ odd). The temperature dependence of the peak intensities of the $(\frac{1}{2}\ \frac{1}{2}\ 1)$ and $(\frac{1}{2}\ \frac{1}{2}\ 3)$ peaks are shown in Fig. 2(a). Also plotted are the integrated intensities of the $(\frac{1}{2}\ \frac{1}{2}\ 1)$ reflection, which match the T dependence of the peak intensity. Figures 2(b) and 2(c) show reciprocal-space scans through the $(\frac{1}{2}\ \frac{1}{2}\ 1)$ peak along the $(HH0)$ and $(00L)$ directions, respectively, at $T = 8$ K and $T = 120$ K. The low temperature peak widths are resolution-limited, indicating long-range order (> 50 Å).

In order to confirm that these peaks originate from magnetic order, we performed polarized neutron measurements. This is the clearest way to distinguish magnetic peaks from weak nuclear superlattice peaks. In general, the elastic magnetic scattering cross section is given by $(\frac{d\sigma}{d\Omega}) \sim \sum_{i,f} |\langle f| \sum_l e^{i\vec{Q}\cdot\vec{r}_l} U_l^{S_i S_f} |i\rangle|^2$, where i and f denote the initial and final states of the system. $U_l^{S_i S_f} \sim F(\vec{Q}) \times \langle S_f | \vec{M}_{\perp l} \cdot \vec{\sigma} | S_i \rangle$ is the scattering amplitude for neutron spin state S_i to S_f at atomic site l, where $F(\vec{Q})$ is the magnetic form factor, $\vec{M}_\perp$ is the component of the magnetic moment perpendicular to the scattering wave vector $\vec{Q}$, and $\vec{\sigma}$ is the spin operator.

We have measured both the spin-flip and non-spin-flip cross sections with neutron polarizations both parallel and perpendicular to the wave vector $\vec{Q}$. Figure 2(d) shows the scattering measured at $T = 8$ K with $\vec{P} \parallel \vec{Q}$ at the $(\frac{1}{2}\ \frac{1}{2}\ 1)$ peak in the (HHL) zone. In this geometry, all magnetic

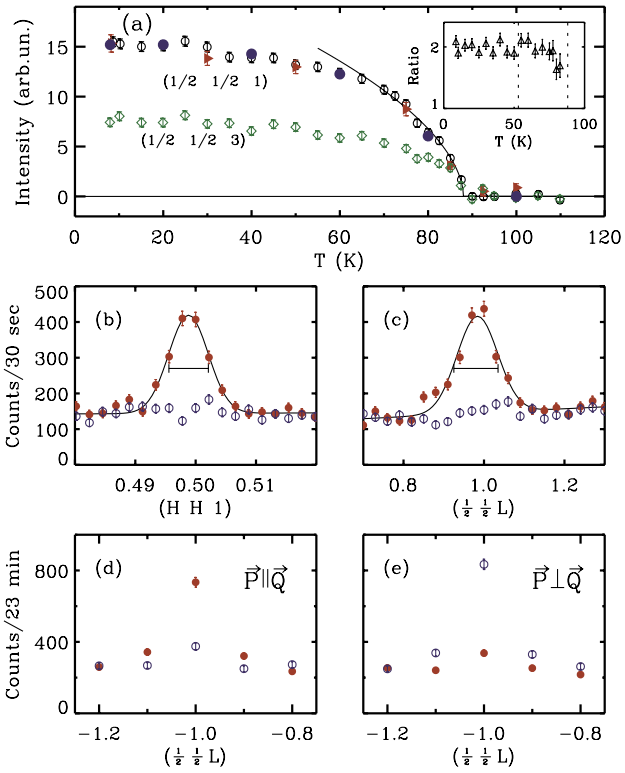

FIG. 2 (color online). (a) Temperature dependence of the intensities at the $(\frac{1}{2}\ \frac{1}{2}\ 1)$ (○) and $(\frac{1}{2}\ \frac{1}{2}\ 3)$ (◇) magnetic Bragg peak positions measured by elastic neutron scattering (a background was subtracted). The filled triangles (▶) denote the integrated intensities obtained from θ scans, and the filled circles (●) denote the intensities measured using polarized neutrons, both scaled to match the 8 K peak intensity of $(\frac{1}{2}\ \frac{1}{2}\ 1)$. The solid line corresponds to $I \propto \langle M \rangle^2 \propto (T_N - T)^{2\beta}$ with $T_N = 88$ K and $\beta = 0.28(1)$. Inset: the ratio of the intensity of $(\frac{1}{2}\ \frac{1}{2}\ 1)$ to that of $(\frac{1}{2}\ \frac{1}{2}\ 3)$. (b) $(HH1)$ scan and (c) $(\frac{1}{2}\ \frac{1}{2}\ L)$ scan through the magnetic $\vec{Q} = (\frac{1}{2}\ \frac{1}{2}\ 1)$ peak at $T = 8$ K (●) and $T = 120$ K (○). The solid lines are Gaussian fits, and the horizontal bars indicate the experimental resolution. The lower panels show polarized neutron data with (d) $\vec{P} \parallel \vec{Q}$ and (e) $\vec{P} \perp \vec{Q}$, for spin-flip (●) and non-spin-flip (○) channels at $T = 8$ K.

scattering occurs in the spin-flip channel, and nuclear scattering is non-spin-flip. The data show that the scattering is entirely spin-flip. The small peak in the non-spin-flip channel is consistent with the background measured at high temperature (not shown), taking into account the instrumental flipping ratio. The temperature dependence of this scattering (scaled to match the unpolarized data at low T) is denoted by the filled circles in Fig. 2(a). We see that the temperature dependence is identical. Thus, the scattering below 88 K at $(\frac{1}{2}\ \frac{1}{2}\ 1)$ is entirely magnetic.

Neutron polarization analysis is also an extremely useful method to deduce the direction of the ordered moment. In Fig. 2(e), we plot the scattering data measured with $\vec{P} \perp \vec{Q}$. The neutron polarization is perpendicular to the (HHL) scattering plane (and hence is perpendicular to the c axis). In this geometry, magnetic scattering can occur in the non-

spin-flip channel if the ordered moment has a component parallel to the polarization direction. If the ordered moment has a large c-axis component, this would lead to a large spin-flip component. Here, the signal predominately occurs in the non-spin-flip channel. Therefore, the direction of the ordered moments lies within the ab plane, and the ordered moment along the c axis must be small (or zero). The error bars on our data allow us to conclude that the size of the c-axis component that contributes to the scattering at $(\frac{1}{2}\ \frac{1}{2}\ 1)$ is less than $\sim 0.04\mu_B$. To further specify the direction of the moments within the plane, the twin domain distribution must be taken into account, as we discuss below. The temperature dependence of the polarized data indicates that the c-axis component remains small at all measured temperatures below $T_N = 88$ K.

The refinement of the magnetic structure is complicated by the presence of multiple twin domains (structural and magnetic). These domains, in principle, can have different populations. To characterize the structural domains, measurements were taken with the sample aligned in the $(HK0)$ zone. Since the Na ion order reduces the sixfold hexagonal symmetry to twofold, there are three possible Na order domains whose relative orientations differ by a rotation of 60° about the c axis. In Fig. 3(a), we show θ scans (which rotate the crystal relative to the incident beam) through peaks at $\vec{Q} = (\frac{1}{2}\ \frac{1}{2}\ 0)$, $(1\ \bar{\frac{1}{2}}\ 0)$, and $(\bar{\frac{1}{2}}\ 1\ 0)$. Each peak is composed of scattering from the Na superlattice of two different structural twin domains. The measured intensities of the peaks are proportional to the populations of the twin domains that contribute to that peak. (We note that part of the intensity variation may be related to neutron absorption by the sample.) The Na order peaks are resolution limited in all three crystallographic directions, indicating that they are macroscopic in size. Also, the relative intensities of these superlattice peaks compared to the fundamental reflections, shown in Table I, indicate that the Na ordering occurs in essentially 100% of our sample.

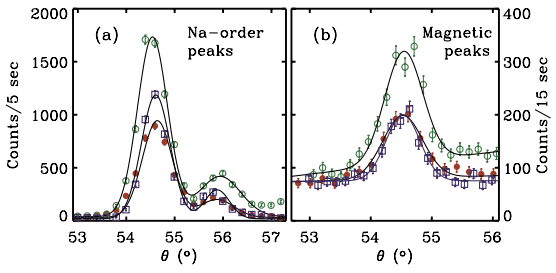

FIG. 3 (color online). (a) Neutron scattering peaks measured in the $(HK0)$ zone at $T = 8$ K. The three sets of data correspond to peaks from three different twin domains due to Na ion ordering: $(\frac{1}{2}\ \frac{1}{2}\ 0)$ (●), $(1\ \bar{\frac{1}{2}}\ 0)$ (○), and $(\bar{\frac{1}{2}}\ 1\ 0)$ (□) (the angle θ was offset by 60° for two of the peaks). The weak peak at ~56° is due to a small crystallite. (b) Magnetic Bragg peaks measured in scattering zones tilted from the $(HK0)$ zone by 14.3° in order to reach the positions $(\frac{1}{2}\ \frac{1}{2}\ 1)$ (●), $(1\ \bar{\frac{1}{2}}\ 1)$ (○), and $(\bar{\frac{1}{2}}\ 1\ 1)$ (□). The solid lines correspond to Gaussian fits.

TABLE I. Observed and calculated integrated intensities of selected nuclear and magnetic Bragg peaks at $T = 8$ K. The $(\frac{1}{2}\ 0\ 1)$ peak was measured using polarized neutrons to separate the magnetic and superlattice intensities. For the $(\frac{1}{2}\ 0\ 3)$ peak, the intensity at $T = 120$ K was subtracted from the intensity at $T = 8$ K. The calculated intensities are based on a model that includes the twin domain distribution, an isotropic Co^{4+} magnetic form factor, and the instrumental resolution function.

(a) Nuclear Bragg peaks			(b) Magnetic Bragg peaks		
Q	$I^{\text{nucl}}_{\text{exp}}$	$I^{\text{nucl}}_{\text{calc}}$	**Q**	$I^{\text{magn}}_{\text{exp}}$	$I^{\text{magn}}_{\text{calc}}$
(1 0 0)	561(12)	603	$(\frac{1}{2}\ \frac{1}{2}\ 1)$	3.9(0.3)	3.5
(0 0 4)	624(27)	568	$(\frac{1}{2}\ \frac{1}{2}\ 3)$	2.2(0.1)	2.3
$(\frac{1}{2}\ \frac{1}{2}\ 0)$	104(9)	96	$(\frac{1}{2}\ \frac{1}{2}\ 5)$	0.6(0.3)	1.2
$(\frac{1}{2}\ 0\ 1)$	29.1(0.9)	30.4	$(\frac{1}{2}\ 0\ 1)$	5.9(0.8)	4.5
$(\frac{1}{2}\ 0\ 2)$	9.2(0.4)	10.0	$(\frac{1}{2}\ 0\ 3)$	3.9(1.6)	3.8

In conjunction with characterizing the structural twins, we have also performed scans through the magnetic positions: $(\frac{1}{2}\ \frac{1}{2}\ 1)$, $(1\ \bar{\frac{1}{2}}\ 1)$, and $(\bar{\frac{1}{2}}\ 1\ 1)$. These scans, shown in Fig. 3(b), were performed by first aligning a $(\frac{1}{2}\ \frac{1}{2}\ 0)$ peak, then tilting the sample by 14.3° to bring the $(\frac{1}{2}\ \frac{1}{2}\ 1)$ position into the horizontal scattering plane. We find that the intensities of these magnetic peaks are proportional to the intensities of the corresponding Na order peaks. This suggests that each structural twin domain corresponds to a magnetic twin domain. That is, the arrangement of ordered magnetic moments appears to be closely coupled to the arrangement of the Na ions, which is a natural expectation due to the symmetry of both arrangements.

The above information on the domain distribution and the moment direction can be combined with measurements of intensities of several nuclear and magnetic Bragg peaks to determine the magnetic structure. Our data are well described by the model shown in Fig. 4. Within each CoO_2 layer, for a single magnetic twin domain, the Co ions are arranged in alternating rows (or stripes) of magnetically ordered and ''nonordered'' ions. For the magnetic ions, the nearest neighbor spins are coupled antiferromagnetically, both along the row and between rows. Between CoO_2 planes, the rows of magnetic Co ions are stacked directly on top of each other, and the nearest neighbor interplane coupling is also antiferromagnetic. The directions of the ordered moments are parallel to the rows. The error bars on our data allow us to put restrictions on the deviations of the ordered moments away from this direction to be less than 10° out of the ab plane. However, within the ab plane, our data are less restrictive, and the moments may be oriented up to 30° away from the stripe direction. The low temperature ($T = 8$ K) static magnetic moment is $0.26(2)\mu_B$ per magnetic Co ion. The size of the observed moment is smaller than that expected for $S = 1/2$, which may suggest the presence of quantum fluctuations or deviations from a fully charge-disproportionated local moment picture.

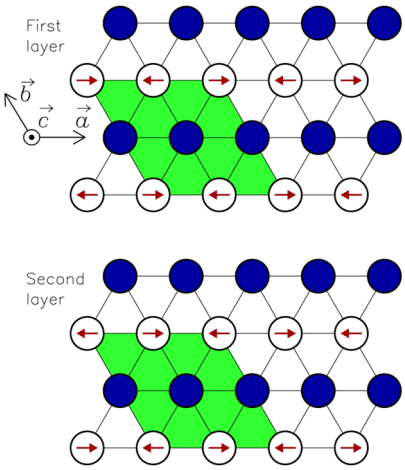

FIG. 4 (color online). Model of the spin arrangement in $Na_{0.5}CoO_2$. The two CoO_2 layers in the magnetic unit cell are depicted, and, for clarity, only Co ions are shown. The solid circles represent "nonordered" Co ions, and the hollow circles represent magnetically ordered Co ions where the arrows indicate the directions of the magnetic moments. The shaded parallelogram outlines the magnetic unit cell.

The structure proposed in Fig. 4 is the simplest model that is consistent with our data, assuming a local moment description of the magnetic order. It is consistent with having rows of Co^{4+} ions that are magnetic (in the $S = 1/2$ low spin state) alternating with rows of Co^{3+} ions (in the $S = 0$ spin state) that are nonmagnetic, as suggested previously [10]. However, we emphasize that our neutron data do not directly probe the valence of the Co ions, only their magnetic moments. For example, the rows of nonordered ions may correspond to Co ions with fluctuating moments, which do not contribute to the long-range antiferromagnetism. The valence difference between the two distinct Co sites may, in fact, be small. Recent NQR studies suggest that unit-valence charge disproportionation does not occur at T_N [16]. It is possible that some degree of valence disproportionation exists already at temperatures above $T_N = 88$ K, and it is primarily the spin components that order at T_N [10]. A delocalized moment model may also describe the data, so long as the periodicity and spin orientation are the same as discussed. The model that we propose differs somewhat from those proposed by Yokoi *et al.* [15]. Their models, obtained from NMR and unpolarized neutron diffraction measurements, involve noncollinear arrangements of two distinct moments with different magnitudes. Although we agree on the fundamental periodicity, our data suggest that the c-axis oriented moments are absent ($< 0.04\mu_B$, as discussed previously).

The anisotropic magnetic susceptibility measurements shown in Fig. 1(c) are consistent with our model. A clear drop is seen at $T_N = 88$ K for $H \parallel ab$, whereas no kink is visible for $H \parallel c$, consistent with the observation that there is essentially no c-axis component to the ordered moment below T_N. The susceptibility data also show an almost isotropic drop below $T = 51$ K, coincident with the upturn in $\rho_{ab}(T)$. A previous μSR study suggested that a spin-reorientation transition occurs near this temperature [17]. We find that there is no indication of this transition in the magnetic neutron scattering. Specifically, the ratio of intensities of the $(\frac{1}{2}\ \frac{1}{2}\ 1)$ and $(\frac{1}{2}\ \frac{1}{2}\ 3)$ Bragg peaks should change if there were a significant spin reorientation below $T = 51$ K, but the inset of Fig. 2(a) shows that the ratio is constant. This is consistent with the polarized neutron results and implies any spin reorientation must be small ($< 10^\circ$ out of the ab plane). Further, this suggests that the drop in susceptibility near $T = 51$ K is not caused by the spins which participate in the antiferromagnetic order below $T_N = 88$ K. Hence, this feature may be related to a gap developing in the excitation spectrum of the "nonordered" Co ions. Finally, the positive magnetoresistance observed below $T_N = 88$ K in Fig. 1(b) can be understood in terms of the orbital motion of charge carriers within this stripe-like ground state. The increased resistivity for $H \parallel c$ may be caused by enhanced scattering for charge motion along one-dimensional chains due to the Lorentz force. Understanding the interplay between spin order and charge motion in this correlated electron system remains an important issue for further study.

We thank P. A. Lee, P. Phillips, and Q. Huang for fruitful discussions. The work at MIT was supported by the Department of Energy under Grant No. DE-FG02-04ER46134 and, in part, by the MRSEC Program of the National Science Foundation under Grant No. DMR 02-13282. J. H. C. was partially supported by the Korea Research Foundation (KRF-2004-005-C00045).

[1] I. Terasaki, Y. Sasago, and K. Uchinokura, Phys. Rev. B **56**, R12 685 (1997).
[2] Y. Wang, N. S. Rogado, R. J. Cava, and N. P. Ong, Nature (London) **423**, 425 (2003).
[3] K. Takada *et al.*, Nature (London) **422**, 53 (2003).
[4] M. L. Foo *et al.*, Phys. Rev. Lett. **92**, 247001 (2004).
[5] H. W. Zandbergen *et al.*, Phys. Rev. B **70**, 024101 (2004).
[6] Q. Huang *et al.*, J. Phys. Condens. Matter **16**, 5803 (2004).
[7] N. L. Wang *et al.*, Phys. Rev. Lett. **93**, 147403 (2004).
[8] J. Hwang, J. Yang, T. Timusk, and F. C. Chou, Phys. Rev. B **72**, 024549 (2005).
[9] K.-W. Lee, J. Kuneš, P. Novak, and W. E. Pickett, Phys. Rev. Lett. **94**, 026403 (2005).
[10] T.-P. Choy, D. Galanakis, and P. Phillips, cond-mat/0502164.
[11] L. Balicas, M. Abdel-Jawad, N. E. Hussey, F. C. Chou, and P. A. Lee, Phys. Rev. Lett. **94**, 236402 (2005).
[12] F. C. Chou, E. T. Abel, J. H. Cho, and Y. S. Lee, J. Phys. Chem. Solids **66**, 155 (2005).
[13] F. C. Chou, J. H. Cho, P. A. Lee, E. T. Abel, K. Matan, and Y. S. Lee, Phys. Rev. Lett. **92**, 157004 (2004).
[14] F. C. Chou, J. H. Cho, and Y. S. Lee, Phys. Rev. B **70**, 144526 (2004).
[15] M. Yokoi *et al.*, J. Phys. Soc. Jpn. **74**, 3046 (2005).
[16] J. Bobroff *et al.*, cond-mat/0507514.
[17] P. Mendels *et al.*, Phys. Rev. Lett. **94**, 136403 (2005).